Making Mn Substitutional Impurities in InAs using a Scanning Tunneling Microscope

Young Jae Song[*†§], *Steven C. Erwin*[¤], *Gregory M. Rutter*[†], *Phillip N. First*[‡], *Nikolai B. Zhitenev*[†], *and Joseph A. Stroscio*[*†]

†Center for Nanoscale Science and Technology, NIST, Gaithersburg, MD 20899

§Maryland NanoCenter, University of Maryland, College Park, MD 20742

¤Center for Computational Materials Science, Naval Research Laboratory, Washington, DC 20375

‡School of Physics, Georgia Institute of Technology, Atlanta, GA 30332

ABSTRACT: We describe in detail an atom-by-atom exchange manipulation technique using a scanning tunneling microscope probe. As-deposited Mn adatoms (Mn_{ad}) are exchanged one-by-one with surface In atoms (In_{su}) to create a Mn surface-substitutional (Mn_{In}) and an exchanged In adatom (In_{ad}) by an electron tunneling induced reaction $Mn_{ad} + In_{su} \rightarrow Mn_{In} + In_{ad}$ on the InAs(110) surface. In combination with density-functional theory (DFT) and high resolution STM imaging, we have identified the reaction pathway for the Mn and In atom exchange.

* Corresponding authors: youngjae.song@nist.gov (YJS); joseph.stroscio@nist.gov (JAS) Center for Nanoscale Science and Technology, NIST, Gaithersburg, MD 20899

One of the great achievements of the scanning tunneling microscope (STM) has been the ability to manipulate single atoms on a surface, in essence extending the human hand into the nanoscale world to manipulate the basic building blocks of matter [1;2]. Different manipulation techniques are chosen by the nature of the interactions between adatoms and substrate/tip materials. The most common manipulation technique is the lateral manipulation method that utilizes a tunable chemical bond interaction between the probe tip and adatom to "slide" the adatom to different lattice sites on the surface [3;4]. This method has been successfully used to create numerous quantum confined nanostructures [5-7]. In adatom-substrate systems where lateral manipulation does not work well, vertical manipulation techniques have been developed. In this approach, the surface adatom is transferred to the probe tip via a voltage pulse, thus breaking the adatom-surface bond. The adatom is transported on the probe tip and released (via another voltage pulse) to a new location anywhere on the surface. An example of this method is the recent creation of novel magnetic nanostructures [8].

Recently, a new type of atom exchange manipulation technique was discovered for Mn adsorbed on GaAs(110) surfaces and used to study Mn-Mn interactions in a dilute magnetic semiconductor [9]. This method was subsequently shown to be applicable to a variety of transition metals on GaAs(110)[10]. In this Letter we shed new light on the details of this manipulation method using the STM to exchange two atoms: a Mn adatom and an In surface atom on the InAs(110) surface. This new method offers some interesting potential applications. In dilute magnetic semiconductors, this exchange reaction can be used to study single impurities with high precision [11], to create tailored interactions between impurities [9], or to investigate spin correlations within more extended "delta-doped" layers constructed atom-by-atom. This manipulation method will also be useful for creating a tailored potential landscape in the two-dimensional electron system that forms on the InAs(110) surface with adatom adsorption [12].

The experiments were performed in a custom-built cryogenic STM system operating at 4.3 K. The InAs(110) surfaces were prepared by cleaving n-type (dopant concentration N_D=1x10^{16} cm^{-3}) bars of InAs in ultra-high vacuum. Ir probe tips prepared by heat treatment and field evaporation in a field-ion microscope were used for tunneling. Mn atoms were deposited on the cleaved InAs surfaces using an

electron-beam evaporator calibrated with a quartz crystal monitor. Mn was deposited at a rate of 0.01 monolayers (ML) per minute on the sample which was cooled to approximately 7 K. At this deposition temperature Mn atoms remain as single adatoms and do not form clusters.

The deposition of Mn adatoms on n-InAs(110) results in a downward band-bending and the formation of a two-dimensional electron gas (2DEG). This implies that Mn_{ad} forms a donor level above the conduction band giving up its electron to the InAs and leaving a positively charged adatom (green arrow, diffuse Mn_{ad} in Fig. 1A). Donor levels above the conduction band are typically found for many metal adatoms on InAs due to the small energy band gap [13]. The positively charged Mn_{ad} will form a screened Coulomb potential around itself resulting in local band bending. As the donor's energy level falls at or below E_F with increased band bending, additional adatoms will not be ionized and the number of ionized Mn_{ad} will saturate. The density of charged adatoms is given by the charge neutrality condition [13]. The 12 % ionization probability observed in this work at a Mn adatom density of 2 x 10^{12} cm^{-2} is similar to that observed for Nb adsorbed on InAs [12].

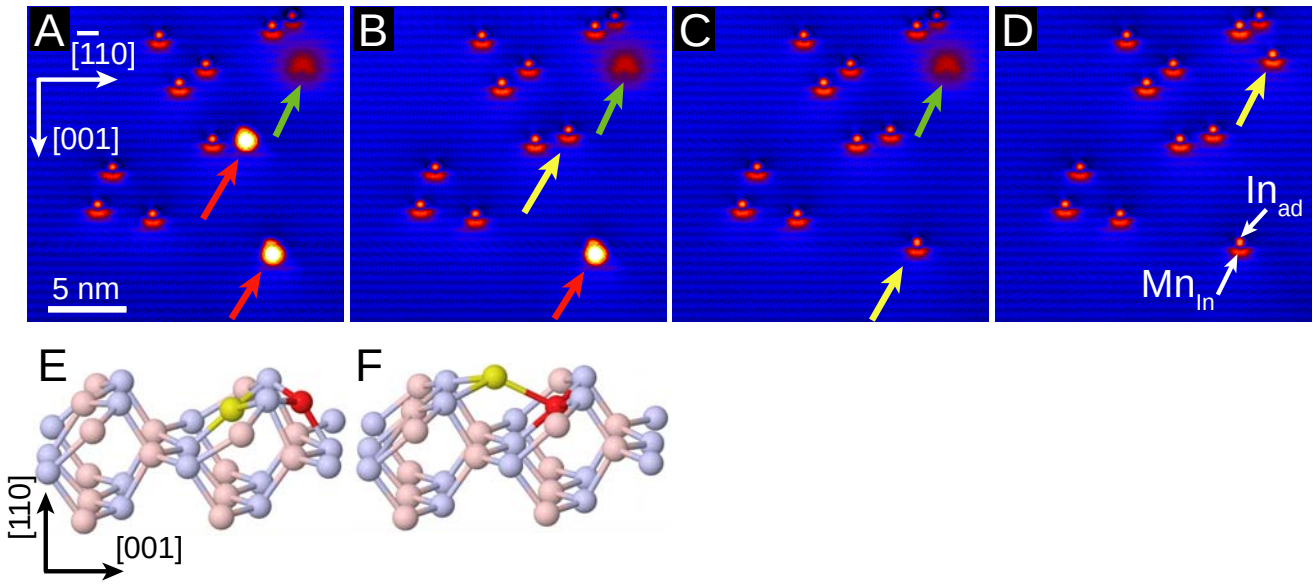

Figure 1: (A-D) Sequence of STM images showing Mn adatoms and Mn-In complexes (crescent shaped features combined with circular features). Red arrows indicate neutral atoms while green arrows indicate ionized atoms. The Mn-In complex consists of a Mn surface-substitutional (Mn_{In}) and an exchanged In adatom (In_{ad}). The image sequence show three tunneling-induced exchange reactions (indicated by yellow arrows), $Mn_{ad} \rightarrow Mn_{In} + In_{ad}$ for the three Mn atoms (two neutral and one ionized). Image size is 20 nm x 20 nm, tunneling current 30 pA, sample bias voltage -1.0V. (E) and (F) show theoretical equilibrium geometries for the initial and final states, respectively, of the exchange reaction. As (blue), In (pink), Mn (red), exchanged In (yellow).

Figure 1A-1D show a series of experimental STM images of atom-by-atom substitutions starting with two different kinds of Mn adatoms to obtain the resultant Mn-In complexes. The two-round shaped features in Fig. 1A (red arrows) are neutral Mn adatoms and the one diffuse feature (green arrow) is a charged (ionized) Mn adatom. In our experiment, the coverage of as-deposited Mn atoms is about 0.0025 ML ($\approx 2 \times 10^{12}$ cm^{-2}), and we observe that approximately 12 % of the Mn atoms are charged at this coverage. As can be seen in the series of images, the STM probe is used to substitute In_{su} with these two types of Mn adatoms (red and green arrows). This final state is identical to the rest of the major features in the image, which were exchanged prior to the taking of this series. The identical nature of the final states gives substantial evidence that both types of adatom features, neutral (red arrow) and charged (green arrow) are derived from Mn adatoms and both types of Mn adatoms are placed one-by-one into the same final state (yellow arrows).

First-principles total-energy calculations were used to determine equilibrium geometries for the initial state ($Mn_{ad} + In_{su}$), final state ($Mn_{In} + In_{ad}$), and the minimum-energy pathway connecting them. Figure 1E shows the initial state with the Mn adatom (red) adsorbed between the InAs surface rows and bonded to multiple As (blue) and In (pink) atoms. The final Mn_{In} state (Fig. 1F) shows the Mn atom substituted for the surface In atom and the In_{ad} (yellow) bridging between two InAs surface rows by bonding to two As atoms and the Mn substitutional. The calculations were performed in a slab geometry with six layers of InAs(110) and a vacuum region of 10 Å. All atomic positions were relaxed, except the bottom InAs layer and its passivating pseudohydrogen layer, until the largest force component on every atom was below 0.05 eV/Å. Total energies and forces were calculated within the Perdew-Burke-Ernzerhof generalized-gradient approximation to DFT using projector-augmented-wave potentials, as implemented in VASP [14-16]. The theoretical minimum-energy pathway between initial and final equilibrium states was calculated using the nudged elastic-band method. The plane-wave cutoff for all calculations was 270 eV. The (110) surface supercell was 2×2 for the total-energy calculations and 4×4 for the STM image simulations; the Brillouin-zone sampling for these supercells was 2×2 and

Γ, respectively. Simulated STM images were calculated using the method of Tersoff and Hamann [17].

The resulting Mn adatom substitution yields Mn-In complexes (crescent plus round features in Fig. 1) consisting of a Mn surface-substitutional atom (Mn_{In}) and an exchanged In adatom (In_{ad}) on the surface. A comparison between a high resolution STM topographic image and the calculated image from DFT for the Mn-In complexes is shown in Figs. 2A and 2B. For the filled-state image in Fig. 2B we integrated the local density of states (LDOS) over a 0.5 eV energy window of occupied states up to the Fermi level. The simulated STM topography under constant-current conditions was then obtained by plotting the height at which the integrated LDOS is constant. Very good agreement is found between theory and experiment for the position of the LDOS intensity in the Mn-In complex. The best agreement with the simulations is with an energy that is slightly lower than the experimental images, presumably due to the voltage drop in the semiconductor. The Mn_{In} in the filled state STM image (Fig. 2A) is dominated by the increased density of states of the two neighboring bonding As atoms. At the position of the Mn_{In} atom in the STM image there appears to be barely any contrast at these tunneling energies. The calculated STM simulation reproduces this increased density of states on the bonded As atoms and the lack of visibility of the Mn substitutional atom. Both experiment and simulation also show prominently the In_{ad} in the images of Figs. 2A and 2B; the circular feature closely matches the geometric position of the In_{ad} found in the equilibrium geometry from the DFT calculations (Fig. 2C).

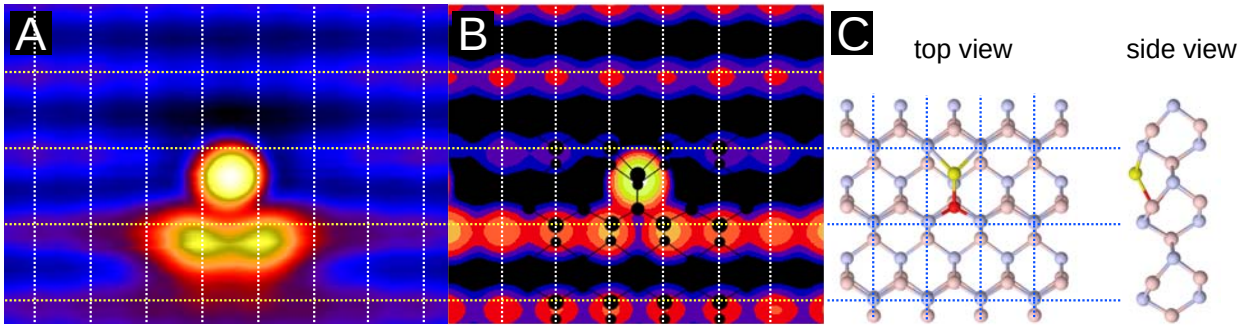

Figure 2: (A) High resolution STM image of the substutional Mn atom and exchanged In adatom on the InAs(110) surface. Image size, 3.4 nm x 2.5 nm, tunneling current 2 nA, sample bias voltage -1.0V. (B) Theoretical simulated STM constant-current topography, at sample bias voltage of -0.5 V, for the configuration depicted in panel C. (C) Equilibrium geometry for the final-state Mn_{In} + In_{ad} complex, as determined from density-functional theory. As (blue), In (pink), Mn (red), exchanged In (yellow).

To investigate the exchange conditions for the Mn adatom with a surface In atom more analytically, we performed current versus voltage (I-V) measurements to pinpoint the threshold voltage by ramping the bias voltage from positive to negative sample potential with the STM tip positioned on top of a Mn adatom (the initial setpoint voltage must be positive to avoid exchanging the atoms). The exchange event can be seen as a dramatic decrease in tunneling current at -0.6 V in the current-voltage measurement (Fig. 3A). The threshold voltage is the same for both the neutral and charged Mn_{ad} adatoms. We find this exchange process to be irreversible, and the repeated I-V measurements after atom exchange do not contain the spike observed in Fig. 3A. For a given tunneling current (and voltage) setpoint, *i.e.* tip-adatom distance, the voltage needed for exchange shows a fairly narrow distribution (Fig. 3B). This result indicates that there is a well-defined threshold voltage or energy required for the exchange process. The observed threshold is weakly dependent on tunneling current setpoint (Fig. 3C) and shows a saturating threshold voltage with a higher setpoint current.

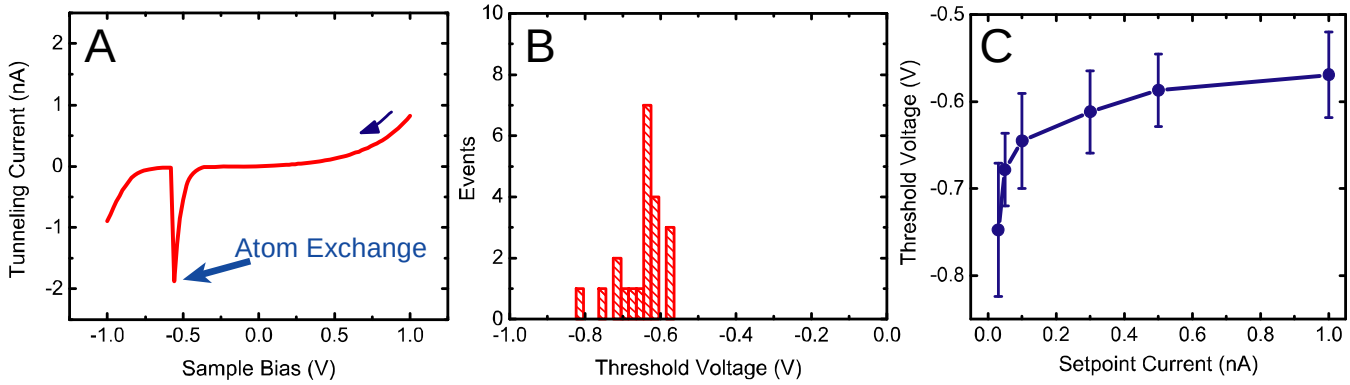

Figure 3: (A) Current-voltage measurements during the Mn and In atom exchange showing the voltage threshold of -0.6 eV for exchange. (B) Histogram of the threshold voltages for atom exchange at 0.1 nA setpoint current. (C) Threshold voltage vs tunneling setpoint current for the Mn and In atom exchange. The error bars represent one standard deviation in the measured distribution in B, which is the dominant contribution to the measurement uncertainty.

We investigated the minimum-energy pathway for the atom exchange reaction using the nudged elastic-band method within DFT. Two low-energy pathways were found: a "kick-out" reaction and a "concerted-exchange" reaction [see online animations]. These two alternatives differ in the direction of

the In atom movement: along $[00\bar{1}]$ for the kick-out reaction, and along [001] for the concerted-exchange reaction. STM imaging shows that the In atom moves in the $[00\bar{1}]$ direction after atom exchange, consistent with the kick-out pathway. Figure 4 shows the energies and corresponding configurations at several points along this pathway. The reaction begins with the Mn_{ad} atom moving down and to the left toward the surface In site. As the Mn atom moves into the In site, the In atom moves in the $[00\bar{1}]$ direction (i.e. to the left in Fig. 4) and upward to bond with the Mn atom and two nearby As atoms. This reaction pathway explains why the tunneling current is dramatically decreased in

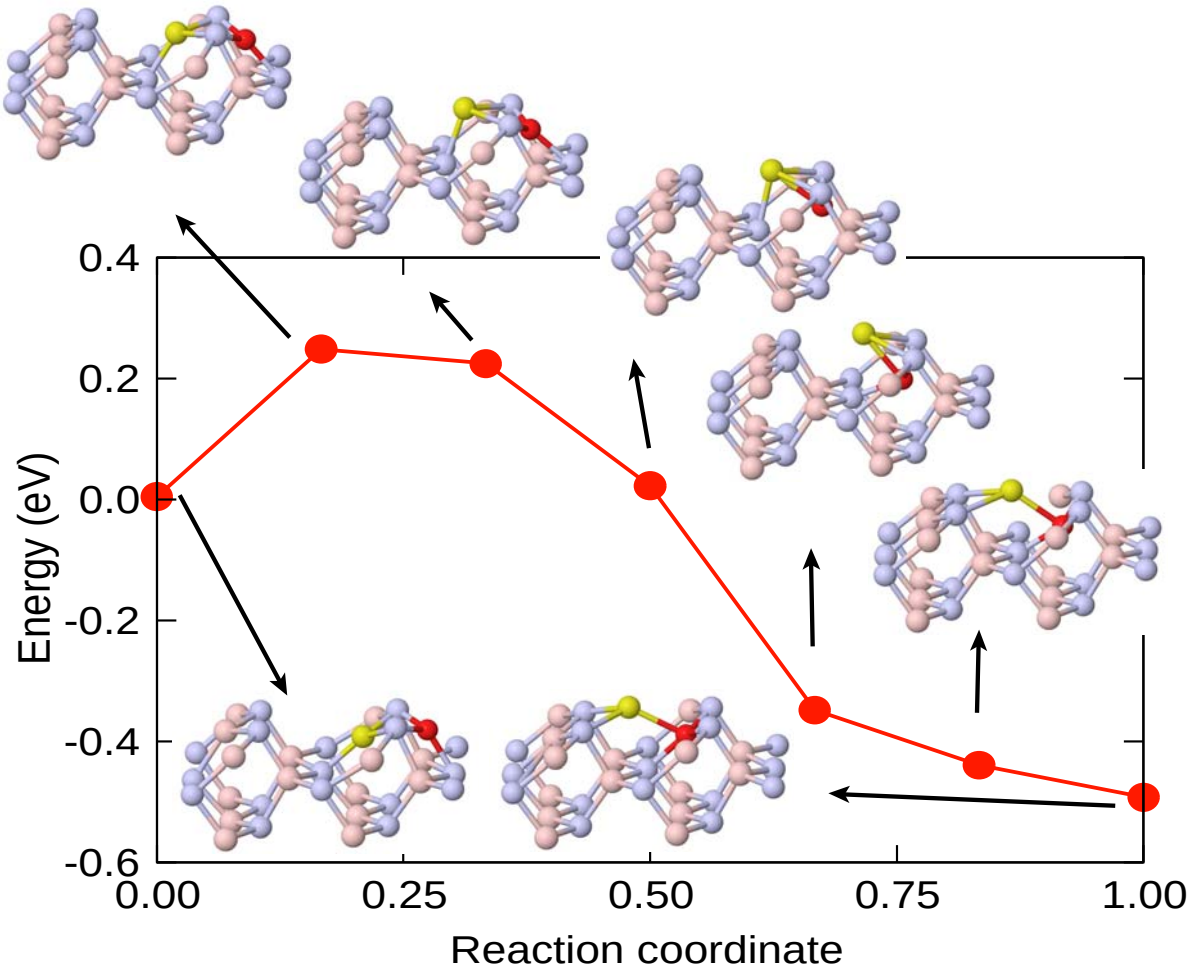

Figure 4: Theoretical minimum-energy pathway for the kick-out reaction $Mn_{ad} \rightarrow Mn_{In} + In_{ad}$. The reaction coordinate describes the motion of both the Mn adatom (red) and its nearest-neighbor surface In atom (yellow). During the reaction the Mn adatom moves leftward and down to become a surface substitutional (Mn_{In}) while the In atom is kicked out, moving leftward and up to become an In adatom (In_{ad}). The reaction pathway and energies were calculated using the nudged elastic-band method within density-functional theory.

the I-V measurement with a fixed tip height, as the Mn atom moves away from the probe tip position. The energy of the configurations show a barrier to the exchange reaction of about 0.3 eV. This agrees favorably with the 0.6 eV threshold found in the STM experiments, which typically overestimates the required energy because of band bending. Interestingly, the calculations show the Mn substitutional to be a lower energy arrangement, implying that the initial Mn_{ad} is a metastable configuration. The lower energy Mn substitutional also explains why the process is irreversible. A similar lower energy state is found for a Mn substitutional impurity in GaAs [18].

The energy-transfer mechanism for the Mn-In atom exchange relies on the tunneling electrons in the STM junction. Previous bond-breaking processes in STM manipulation experiments have been discussed using vibrational excitations via inelastic electron tunneling [3;19-22]. Depending on the exact nature of the vibrational coupling, multiple low-energy excitations or a single high-energy excitation can induce bond-breaking events. The observation of a clear threshold is indicative of a single electron process [21;22]. The rather high energies observed for the Mn-In exchange compared with vibrational excitations indicate that a more direct electronic excitation is likely responsible for the manipulation [23]. The reaction yield and its dependence on tunneling current and voltage can typically give clues to the process; however, in the case of an irreversible process, such measurements of yield are difficult. The Mn-In exchange is observed to occur only when electrons are tunneling from the InAs into the probe tip at negative sample potential and is not observed at positive potentials. This likely rules out a vibrational excitation mechanism, which would be independent of polarity. A single polarity excitation process may be associated with the electric field polarity in the tunneling junction or may depend on the location of a particular energy level. In our work, the field strength for each threshold voltage (threshold voltage divided by tip-sample distance) is about 5.6×10^6 Vcm^{-1}, which is two orders of magnitude lower than the normal field evaporation strength [24]. On the other hand, our DFT calculations reveal a minority-spin state close to the valence band maximum which may play a role in the exchange process. STM induced Mn-In exchange measurements with spin-polarized tunneling may give some insight into this process in future measurements.

In summary, we have shown that the exchange of Mn and In atoms at the InAs(110) surface can be induced with the scanning tunneling microscope. The exchange process occurs only when tunneling out of the InAs surface in excess of a voltage threshold of -0.6 V to create a substitutional Mn impurity atom. Density-functional theory calculations have determined the minimum energy reaction pathway, in which the In atom is kicked out by the substitution of a Mn atom into the In site. This occurs with an energy barrier of 0.3 eV, and has lower energy in the final state than the Mn adatom on the surface making it an irreversible process. We believe this new exchange manipulation method will be very useful for future studies in nanomagnetism/spintronics and to low-dimensional electron systems with tailored impurity potentials.

Acknowledgements: This work was supported in part by the Korean Research Foundation, the Office of Naval Research, and the NIST-CNST/UMD-NanoCenter Cooperative Agreement. Computations were performed at the DoD Major Shared Resource Center at AFRL. We thank Young Kuk, Mark Stiles, and Anthony Richardella for valuable comments, and Nathan Guisinger, Steve Blankenship, Alan Band, Dave Rutter, and Frank Hess for technical assistance.

Supporting Information Available (web enhanced objects). Two animations which show the reaction pathways discussed in the text are available on line, filenames: kick_out.qt and concerted_exchange.qt. This material is available free of charge via the Internet at http://pubs.acs.org.

FIGURE CAPTIONS

Figure 1: (A-D) Sequence of STM images showing Mn adatoms and Mn-In complexes (crescent shaped features combined with circular features). Red arrows indicate neutral atoms while green arrows indicate ionized atoms. The Mn-In complex consists of a Mn surface-substitutional (Mn_{In}) and an exchanged In adatom (In_{ad}). The image sequence show three tunneling-induced exchange reactions (indicated by yellow arrows), $Mn_{ad} \rightarrow Mn_{In} + In_{ad}$ for the three Mn atoms (two neutral and one ionized). Image size is 20 nm x 20 nm, tunneling current 30 pA, sample bias voltage -1.0V. (E) and (F) show

theoretical equilibrium geometries for the initial and final states, respectively, of the exchange reaction. As (blue), In (pink), Mn (red), exchanged In (yellow).

Figure 2: (A) High resolution STM image of the substitutional Mn atom and exchanged In adatom on the InAs(110) surface. Image size, 3.4 nm x 2.5 nm, tunneling current 2 nA, sample bias voltage -1.0V. (B) Theoretical simulated STM constant-current topography, at sample bias voltage of -0.5 V, for the configuration depicted in panel C. (C) Equilibrium geometry for the final-state Mn_{In} + In_{ad} complex, as determined from density-functional theory. As (blue), In (pink), Mn (red), exchanged In (yellow).

Figure 3: (A) Current-voltage measurements during the Mn and In atom exchange showing the voltage threshold of -0.6 eV for exchange. (B) Histogram of the threshold voltages for atom exchange at 0.1 nA setpoint current. (C) Threshold voltage vs tunneling setpoint current for the Mn and In atom exchange. The error bars represent one standard deviation in the measured distribution in B, which is the dominant contribution to the measurement uncertainty.

Figure 4: Theoretical minimum-energy pathway for the kick-out reaction $Mn_{ad} \rightarrow Mn_{In} + In_{ad}$. The reaction coordinate describes the motion of both the Mn adatom (red) and its nearest-neighbor surface In atom (yellow). During the reaction the Mn adatom moves leftward and down to become a surface substitutional (Mn_{In}) while the In atom is kicked out, moving leftward and up to become an In adatom (In_{ad}). The reaction pathway and energies were calculated using the nudged elastic-band method within density-functional theory.

Reference List

(1) Eigler, D. M.; Schweizer, E. K. *Nature* **1990**, *344*, 524-526.

(2) J.A.Stroscio; D.M.Eigler *Science* **1991**, *254*, 1319-1326.

(3) J.A.Stroscio; R.J.Celotta *Science* **2004**, *306*, 242-247.

(4) L.Bartels; G.Meyer; K.-H Rieder *Physical Review Letters* **1997**, *79*, 697.

(5) Crommie, M. F.; Lutz, C. P.; Eigler, D. M. *Science* **1993**, *262*, 218-220.

(6) Manoharan, H. C.; Lutz, C. P.; Eigler, D. M. *Nature* **2000**, *403*, 512-515.

(7) Heinrich, A. J.; Lutz, C. P.; Gupta, J. A.; Eigler, D. M. *Science* **2002**, *298*, 1381-1387.

(8) Hirjibehedin, C. F.; Lutz, C. P.; Heinrich, A. J. *Science* **2006**, *312*, 1021-1024.

(9) Kitchen, D.; Richardella, A.; Tang, J. M.; Flatte, M. E.; Yazdani, A. *Nature* **2006**, *442*, 436-439.

(10) Richardella, A.; Kitchen, D.; Yazdani, A. *Physical Review B* **2009**, *80*, 045318.

(11) Garleff, J. K.; Celebi, C.; Van Roy, W.; Tang, J. M.; Flatte, M. E.; Koenraad, P. M. *Physical Review B* **2008**, *78*.

(12) Getzlaff, M.; Morgenstern, M.; Meyer, C.; Brochier, R.; Johnson, R. L.; Wiesendanger, R. *Physical Review B* **2001**, *63*.

(13) Monch, W. *Semiconductor Surfaces and Interfaces*; Springer-Verlag: Berlin, 2001.

(14) Kresse, G.; Hafner, J. *Physical Review B* **1993**, *47*, 558.

(15) Kresse, G.; Furthmuller, J. *Physical Review B* **1996**, 11169.

(16) disclamer. The full description of the procedures used in this paper requires the identification of certain commercial products and their suppliers. The inclusion of such information should in no way be construed as indicating that such products or suppliers are endorsed by NIST or are recommended by NIST or that they are necessarily the best materials, instruments, software or suppliers for the purposes described.

(17) Tersoff, J.; Hamann, D. R. *Physical Review B* **1985**, *31*, 805.

(18) Fu, H. X.; Ye, L.; Zhang, K. M.; Xide, X. *Surface Science* **1995**, *341*, 273-281.

(19) Shen, T. C.; Wang, C.; Abeln, G. C.; Tucker, J. R.; Lyding, J. W.; Avouris, P.; Walkup, R. E. *Science* **1995**, *268*, 1590-1592.

(20) Gao, S. W.; Persson, M.; Lundqvist, B. I. *Physical Review B* **1997**, *55*, 4825-4836.

(21) Ueba, H. *Surface Review and Letters* **2003**, *10*, 771-796.

(22) Stroscio, J. A.; Tavazza, F.; Crain, J. N.; Celotta, R. J.; Chaka, A. M. *Science* **2006**, *313*, 948-951.

(23) M.Lastapis; M.Martin; D.Riedel; L.Hellner; G.Comtet; G.Dujardin *Science* **2005**, *308*, 1000-1003.

(24) Muller, W.; Tsong, T. T. *Field Ion Microscopy, Principles and Applications*; Elsevier: New York, 1969.